

Solitons supported by a self-defocusing trap in a fractional-diffraction waveguide

Mateus C. P. dos Santos^{a,*}, Boris A. Malomed^{b,c}, Wesley B. Cardoso^a

^aInstituto de Física, Universidade Federal de Goiás, 74.690-970, Goiânia, Goiás, Brazil

^bDepartment of Physical Electronics, School of Electrical Engineering, Faculty of Engineering, and Center for Light-Matter Interaction, Tel Aviv University, P.O.B. 39040, Tel Aviv, Israel

^cInstituto de Alta Investigación, Universidad de Tarapacá, Casilla 7D, Arica, Chile

Abstract

We introduce a model which gives rise to self-trapping of fundamental and higher-order localized states in a one-dimensional nonlinear Schrödinger equation with fractional diffraction and the strength of the self-defocusing nonlinearity growing steeply enough from the center to periphery. The model can be implemented in a planar optical waveguide. Stability regions are identified for the fundamental and dipole (single-node) states in the plane of the Lévy index and the total power (norm), while states of higher orders are unstable. Evolution of unstable states is investigated too, leading to spontaneous conversion towards stable modes with fewer node.

Keywords: Fractional nonlinear Schrödinger equation, Stability analysis, Localized solutions, Defocusing nonlinearity, Spatial soliton

1. Introduction

The fractional Schrödinger equation (FSE) was first introduced by N. Laskin for wave function Ψ of a quantum particle moving by Lévy flights. [1–3]. In the scaled form, with time t and coordinate x , the one-dimensional FSE derived in those works is (see also Ref. [4])

$$i\frac{\partial\Psi}{\partial t} = \frac{1}{2} \left(-\frac{\partial^2}{\partial x^2} \right)^{\alpha/2} \Psi + V(x)\Psi, \quad (1)$$

where $V(x)$ is the usual potential which appears in the usual Schrödinger equation. The kinetic-energy operator in Eq. (1), with the Lévy index (LI) α , which may take values

$$0 < \alpha \leq 2, \quad (2)$$

[5], is represented by the fractional *Riesz derivative* [6, 7], which is defined as the juxtaposition of the direct and inverse Fourier transforms [8–10],

$$\left(-\frac{\partial^2}{\partial x^2} \right)^{\alpha/2} \Psi = \frac{1}{2\pi} \int_{-\infty}^{+\infty} dp |p|^\alpha \int_{-\infty}^{+\infty} d\tilde{\xi} e^{ip(x-\tilde{\xi})} \Psi(\tilde{\xi}), \quad (3)$$

where p is the Fourier-space wavenumber conjugate to coordinate x . The limit value $\alpha = 2$ corresponds to the usual (non-fractional) kinetic-energy operator, $-\partial^2/\partial x^2$.

Proceeding from the single-particle FSE (1), one may attempt to introduce its generalization in the form of the

Gross-Pitaevskii equation [11] for the Bose-Einstein condensate in an ultracold gas of Lévy-flying particles:

$$i\frac{\partial\Psi}{\partial t} = \frac{1}{2} \left(-\frac{\partial^2}{\partial x^2} \right)^{\alpha/2} \Psi + V(x)\Psi + \sigma|\Psi|^2\Psi, \quad (4)$$

where $\sigma = +1$ or -1 corresponds to repulsive or attractive contact interactions, respectively, between the particles [12, 13]. However, a consistent derivation of the fractional Gross-Pitaevskii equation in the framework remains a challenging problem.

Realizations of the fractional quantum mechanics were also proposed in solid-state Lévy crystals [14] and exciton-polariton condensates in semiconductor microcavities [15]. However, no experimental demonstration of fractional quantum systems has been demonstrated, as yet.

A more feasible approach to the physical realization of FSEs in the form of classical equations is suggested by the commonly known similarity of the Schrödinger equation in quantum mechanics and the propagation equation for the optical field under the condition of paraxial diffraction, with time t replaced in Eq. (1) by the propagation distance, z , which plays the role of the evolution variable in optical waveguides [16]. A scheme for the realization of this possibility was proposed by Longhi [17], in terms of the transverse light dynamics in optical cavities with the 4f (four-focal-lengths) structure. The proposed setup incorporates two lenses and a phase mask, which is placed in the middle (Fourier) plane. The first lens performs decomposition of the light beam into Fourier components, with respect to the transverse coordinates, while the second lens recombines the component back into a single beam. The action of the fractional diffraction is

*Corresponding author

Email addresses: mateuscalixtopereira@gmail.com (Mateus C. P. dos Santos), malomed@tauex.tau.ac.il (Boris A. Malomed), wesleybcardoso@ufg.br (Wesley B. Cardoso)

emulated, in the Fourier plane, by the corresponding differential phase shifts imposed by the phase mask. The scheme may also include a curved mirror placed at an edge of the cavity, which introduces a phase shift representing potential $V(x)$ in Eq. (1).

Experimental implementation of such an optical setup has not been reported as yet. However, effective fractional group-velocity dispersion has been recently realized in a fiber-laser scheme [18].

Once the FSE may be implemented as the propagation equation in optics, a natural possibility is to include the self-focusing or defocusing nonlinearity of the optical material. The respective fractional nonlinear Schrödinger equation (FNLSE) for amplitude $U(x, z)$ of the electromagnetic wave is [12, 19, 20]

$$i \frac{\partial}{\partial z} U = \frac{1}{2} \left(-\frac{\partial^2}{\partial x^2} \right)^{\alpha/2} U + \eta |U|^2 U, \quad (5)$$

where η is the nonlinearity coefficient, and the external potential is neglected. The regular (non-fractional) diffraction corresponds to $\alpha = 2$ [2, 4]. In the case of self-focusing, which corresponds to $\eta < 0$ in Eq. (5), the FNLSE (5) gives rise to a family of *fractional solitons* [21–25], see also review [12]. They exist in the interval of $1 < \alpha \leq 2$, as the same FNLSE gives rise to the *collapse* at $\alpha < 1$ [12]. On the other hand, the collapse does not take place in the case of self-defocusing, which corresponds to $\eta > 0$ in Eq. (5) and is the subject of the present work. Therefore, we here consider the full interval (2). Recently, nonlinear modes in the form of *domain walls* were studied in a system of two coupled FNLSEs with the self-repulsive nonlinearity, in the full interval of $0 < \alpha \leq 2$ [26].

A possibility to produce soliton-like modes in nonlinear Schrödinger equations with the defocusing nonlinearity was proposed in Refs. [27–33]. It makes use of spatial modulation of the nonlinearity strength, growing steeply enough from the center to periphery, which gives rise to self-trapping of various one- and two-dimensional localized modes. The objective of the work is to investigate this possibility in the one-dimensional setting with the fractional diffraction. The model is introduced in Section 2. Results of systematic numerical investigation of fundamental and higher-order self-trapped states are summarized in Section 3, the most important results concerning stability of these states. The paper is concluded by Section 4.

2. The model

We consider an optical beam propagating in a planar waveguide with self-defocusing nonlinearity and fractional diffraction. The evolution of amplitude $U(z, t)$ of the optical field is governed by the FNLSE. In the rescaled form, it takes the form,

$$i \frac{\partial}{\partial z} U = \frac{1}{2} \left(-\frac{\partial^2}{\partial x^2} \right)^{\alpha/2} U + \eta(x) |U|^2 U, \quad (6)$$

where z is the normalized propagation distance and x the transverse coordinate. The fractional diffraction with LI α [5] is represented in Eq. (6) by the Riesz derivative [6, 7]. It is defined, in terms of the Fourier-transform operator \mathcal{F} , as [8–10]

$$\left(-\frac{\partial^2}{\partial x^2} \right)^{\alpha/2} U(x, z) = \mathcal{F}^{-1} \{ |\omega|^\alpha \mathcal{F}[U(x, z)] \}, \quad (7)$$

where ω is the wavenumber in the Fourier space conjugate to coordinate x .

Here, we assume that the self-trapping of localized states is provided by local modulation of the defocusing cubic nonlinearity, defined in Eq. (6) by coefficient $\eta(x) > 0$ with a minimum at $x = 0$, which grows steeply enough at $|x| \rightarrow \infty$. The creation of various stable soliton-like modes by means of the nonlinear potential well induced by the appropriate profile of $\eta(x)$ in the case of the regular diffraction ($\alpha = 2$) was elaborated in Refs. [27–29, 32]. Such modes with propagation constant $b < 0$ are looked for as

$$U(x, z) = e^{ibz} u(x), \quad (8)$$

with real function u satisfying the equation

$$bu + \frac{1}{2} \left(-\frac{\partial^2}{\partial x^2} \right)^{\alpha/2} u + \eta(x) u^3 = 0. \quad (9)$$

The asymptotic form of the solution to Eq. (9) at $|x| \rightarrow \infty$ is correctly produced by the Thomas-Fermi approximation, which neglects the diffraction term in the equation [34],

$$u_{\text{TF}}^2(x) = -b/\eta(x). \quad (10)$$

As it follows from Eq. (10), the condition necessary for the convergence of the soliton's total power (norm), which is a dynamical invariant of Eq. (6),

$$P = \int_{-\infty}^{+\infty} u^2(x) dx, \quad (11)$$

is that $\eta(x)$ grows at $|x| \rightarrow \infty$ faster than $|x|$. In most works [27–29, 32], the modulation is adopted in a steeper form – in particular, as

$$\eta(x) = \cosh^2(x), \quad (12)$$

which we adopt here. In optics, such modulation formats may be realized by means of the spatially inhomogeneous distribution of dopants resonantly interacting with the light beam, or by a spatially inhomogeneous profile of the resonance detuning in the dopants [35, 36].

The stability of static solutions (8) is addressed by means of linearized equations for small perturbations, taking a solution as

$$U_p(x, z) = e^{ibz} \left[u(x) + v(x)e^{\lambda z} + w^*(x)e^{\lambda^* z} \right], \quad (13)$$

where $v(x)$ and $w(x)$ are components of the eigenmode of the perturbation and λ is an eigenvalue (that may be

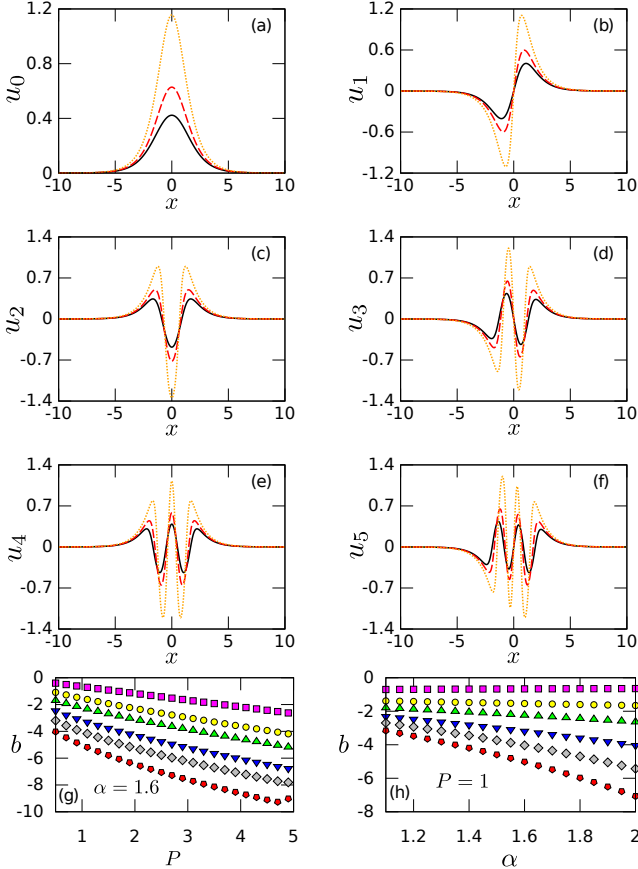


Figure 1: Profiles of bound states: (a) u_0 , (b) u_1 , (c) u_2 , (d) u_3 , (e) u_4 , and (f) u_5 , as produced by the numerical solution of Eq. (9), with LI $\alpha = 1.6$, based on the relaxation method. The profiles with powers $P = 0.5, 1$ and 3 are displayed by solid (black), dashed (red) and dotted (orange) lines, respectively. Panels (g) and (h) display, severally, the propagation constant b vs. P for fixed $\alpha = 1.6$, and b vs. α for fixed $P = 1$, by means of squares (magenta), circles (yellow), triangles (green), inverted triangles (blue), diamonds (gray), and hexagons (red), which correspond to the states u_0, u_1, u_2, u_3, u_4 and u_5 , respectively.

complex), the stability condition being $\text{Re}(\lambda) = 0$ for all eigenvalues. To substitution of expression (13) U_p into Eq. (6) and linearization with respect to $v(x)$ and $w(x)$ leads to the eigenvalue problem,

$$-i \begin{bmatrix} C_1 & C_2 \\ -C_2 & -C_1 \end{bmatrix} \begin{bmatrix} v \\ w \end{bmatrix} = \lambda \begin{bmatrix} v \\ w \end{bmatrix}, \quad (14)$$

where we define

$$C_1 \equiv \frac{1}{2} \left(-\frac{\partial^2}{\partial x^2} \right)^{\alpha/2} + b + 2\eta u^2, \quad (15)$$

$$C_2 \equiv \eta u^2. \quad (16)$$

The problem based on Eq. (14) can be solved by means of the Fourier collocation method [37].

3. Numerical results

The ground-state and higher-order (excited) stationary solutions of Eq. (6), u_n , with $n = 0, 1, 2, \dots$, where

n is the number of nodes in $u_n(z)$, were found by means of the well-known imaginary-time evolution method [38]. This procedure was implemented using the split-step algorithm based on the Fourier spectral method with numerical steps $\Delta_x = 0.04$ and $\Delta_z = 0.001$. Hermite-Gaussian functions were employed as the natural input profiles. In the numerical calculations, the higher-order modes, with $n \geq 1$, are obtained using the Gram-Schmidt orthogonalization process, performed at each integration step [32]. Alternatively, all these modes can be obtained by means of the relaxation method, using the same input profiles.

To study the stability and dynamics of the stationary states, we calculated the spectrum of perturbation eigenvalues and verified the corresponding predictions for the stability, running real-time simulations of the perturbed evolution.

First, examples of the family of solutions with $n = 0, 1, 2, 3, 4$ and 5 , for LI $\alpha = 1.6$ and powers $P = 0.5, 1$ and 3 [see Eq. (11)], are displayed in Figs. 1(a)-1(f), where we observe that the increase in the power naturally produces solutions with larger amplitudes, maintaining the number of nodes. In Figs. 1(g) and 1(h) the results are summarized by dependences $b(P)$ for fixed $\alpha = 1.6$ and $b(\alpha)$ for fixed $P = 1$. We observe, in particular, that all families of stationary states satisfy the *anti-Vakhitov-Kolokolov* criterion, $db/dP < 0$. It is a necessary condition for the stability of localized states supported by a self-defocusing nonlinear term [39] (the Vakhitov-Kolokolov criterion per se, $db/dP > 0$, is a well-known stability condition for solitons in the case of self-focusing [40–42]). On the other hand, the lowest modes u_n , with $n = 0$ and 1 , demonstrate a very weak dependence of their propagation constants on LI, the dependence getting conspicuous ($db/d\alpha < 0$) for $n \geq 2$. This finding is explained by the fact that the above-mentioned TF approximation, which ignores the derivative term in Eq. (6), plays a dominant role for the modes with the simplest structure, while more sophisticated ones, with a larger number of nodes, are sensitive to the diffraction effect, i.e., to α . The negative sign of $db/d\alpha$ is explained by the fact that, around the peaks in the shape of $|u_n(x)|$, the sign of the curvature is opposite to the sign of $u_n(x)$ of the trapped state, therefore the diffraction term makes a negative contribution to b , with the size growing with the increase of P .

Proceeding to the stability analysis of the bound states, in Figs. 2(a) and 2(b) we plot, severally, largest real parts of the stability eigenvalues produced by the numerical solution of Eq. (14), as functions of α for $P = 1$, and as functions of P for fixed $\alpha = 1.6$, for the self-trapped modes u_n with $n = 0, 1, 2$ and 3 . We observe that the nodeless ground-state modes, u_0 , with $P = 1$ are completely stable for $\alpha > 0.28$. This is not the same for the higher-order modes. The one with $n = 1$ features a restricted stability region, $\alpha > \alpha_{\min}^{(n=1)} \approx 1.61$, while the modes $n > 1$ are completely unstable at all values of $\alpha < 2$.

Another essential result is the analysis of the stabil-

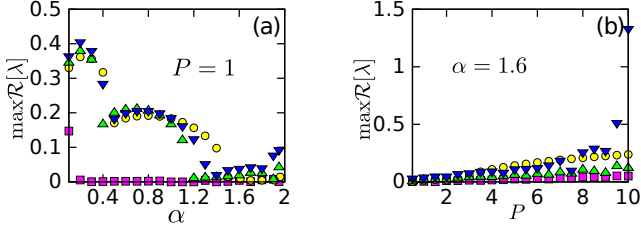


Figure 2: The maximum value of the instability growth rate, $\text{Re}(\lambda)$, for the bound states, as a function of α (a) and P (b). $\text{Re}(\lambda)$ is produced by the numerical solution of Eq. (14). The results for the bound states u_0 , u_1 , u_2 , and u_3 are presented by squares (magenta), circles (yellow), triangles (green), and inverted triangles (blue), respectively.

ity as a function of the power, for a fixed value of LI. Indeed, in Fig. 2(b), we observe that the increase in P leads to destabilization of modes. For the case with $\alpha = 1.6$, as shown in Fig. 2(b), the self-trapped nodeless mode is not stable for all values of P , presenting instability for $P > 2.8$. The same behavior is observed for the mode u_1 . Similar to the case shown in Fig. 2(a), no stability region is found for modes with $n > 1$ (although it is seen in Fig. 2(a) that the instability of the states with $n = 2$ is very weak). The latter conclusion pertains as well to the case of the normal (non-fractional) diffraction, $\alpha = 2$. In this connection, it is relevant to mention that, in the case of the still steeper *anti-Gaussian* modulation of the local self-defocusing strength, rather than the profile (12) adopted here, the state with $n = 2$ is stable too at $\alpha = 2$, while the instability commences from $n = 3$. The complex behavior of the stability region of the bound states, considering the variations of α and P , is studied in detail below, and the results are shown in Fig. 6.

To verify the predictions for the stability and instability of the bound states produced by the linear-stability analysis, we have performed direct simulations using as input the numerically obtained stationary solutions with amplitudes randomly perturbed at the $\pm 3\%$ level. Absorbing boundary conditions were applied at edges of the integration domain to preclude artifacts produced by reflected radiation waves. The numerical solution performed with the edge absorbers may break the conservation of the power, defined by Eq. (11), which would be one of indicators for the instability of the underlying stationary solution.

Figure 3 displays the perturbed evolution of the bound states u_0 , u_1 , u_2 and u_3 for $\alpha = 1.7$ and $P = 1$. It is seen that u_0 and u_1 demonstrate full dynamical stability. On the other hand, modes u_n with $n \geq 2$ exhibit instabilities. In particular, u_2 displays nonperiodic oscillations of its amplitude. The evolution of u_3 shows a more dramatic unstable behavior, in which the initial profile with three nodes abruptly transforms into the zero-node one. In all the cases, the results are in agreement with the stability/instability predictions produced by the eigenvalues of small perturbations, cf. see Fig. 2.

The evolution of the total power corresponding to the

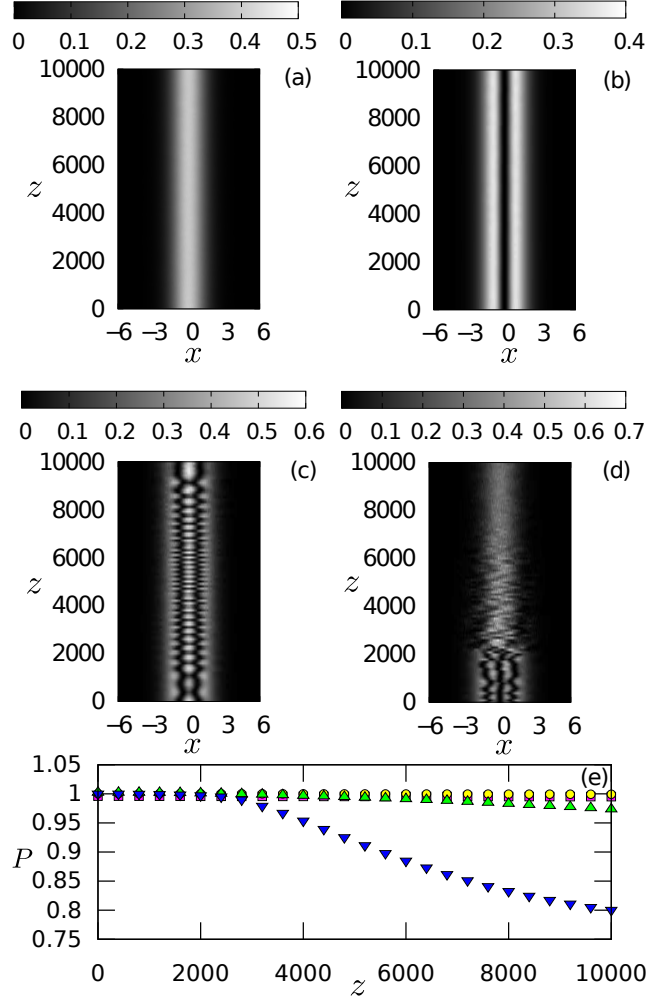


Figure 3: The evolution of the perturbed modes with $\alpha = 1.7$ and $P = 1$. The results are presented for (a) $|u_0|^2$, (b) $|u_1|^2$, (c) $|u_2|^2$, and (d) $|u_3|^2$. Panel (e) displays the total power versus z for the cases shown in panels (a-d), displayed by squares (magenta), circles (yellow), triangles (green), and inverted triangles (blue) for u_0 , u_1 , u_2 and u_3 , respectively.

same cases is shown in Fig. 3(e). The power of the stable states ($u_{0,1}$) remains constant, while the unstable configurations demonstrate losses, due to the above-mentioned effect of the elimination of developing perturbations by the boundary absorbers. In particular, mode u_3 loses 20% of the initial power loss by $z = 10^4$. Eventually, the remaining state converges to a nodeless single-peak ground state, which keeps $\approx 70\%$ of the initial power. In general, higher-order unstable modes with larger values of α (stronger diffraction) tend to show more abrupt power loss which commences earlier.

The effect of LI on the stability of the bound states is presented in Fig. 4, which displays the evolution of the states similar to those in Fig. 3, but with a smaller LI, $\alpha = 1.2$. In this case, the nodeless ground state remains completely stable. On the other hand, the u_1 mode is now unstable, in contrast with its counterpart shown above for $\alpha = 1.7$. The instability development abruptly transforms its shape from the single-node one into a robust nodeless

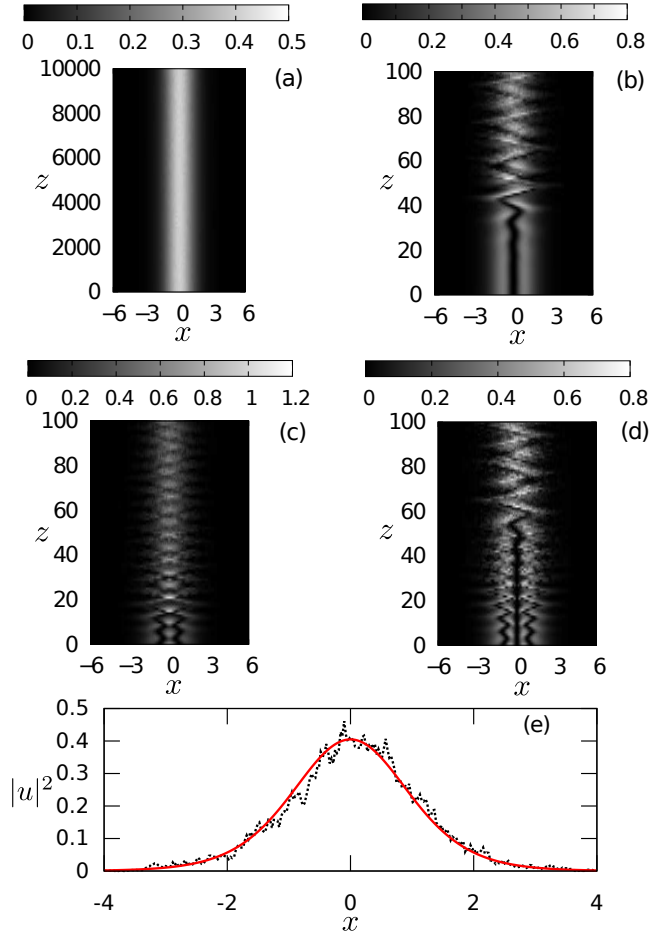


Figure 4: Panels (a)-(d) display the same as in Figs. 3(a)-3(d), but for $\alpha = 1.2$. (e) Comparison between the intensity of the nodeless ground state $|u_0|^2$ (the solid line) and the output produced by the perturbed evolution (spontaneous conversion) of the first-order mode $|u_1|^2$ at $z = 9600$ (the dotted line).

one. This result may be identified as spontaneous transformation of the unstable u_1 state into the stable ground state u_0 , as shown in Fig. 4(e). In this case ($\alpha = 1.2$), all excited states u_n with $n \geq 1$ are unstable, indicating that the decrease of α , i.e., weaker fractional diffraction, leads to destabilization of the excited states. In some cases, the instability triggers a more complex spontaneous evolution. For example, unstable mode u_3 transforms first to u_2 , before converging later to the nodeless mode. On the other hand, the instability-driven evolution in the case of lower values α does not exhibit conspicuous power loss, i.e., the weaker fractional diffraction gives rise to very weak emission of radiation.

We have also verified how the perturbed evolution of modes depends on total power, P , confirming the predictions of the linear-stability analysis indicate that the increase in P should lead to destabilization. A example of the evolution of modes u_0 and u_1 is displayed in Fig. 5, for the same configurations as in Fig. 3, but with high values of P . In particular, the unstable evolution of the nodeless mode is observed at $\alpha = 1.7$ and $P = 10$. In this

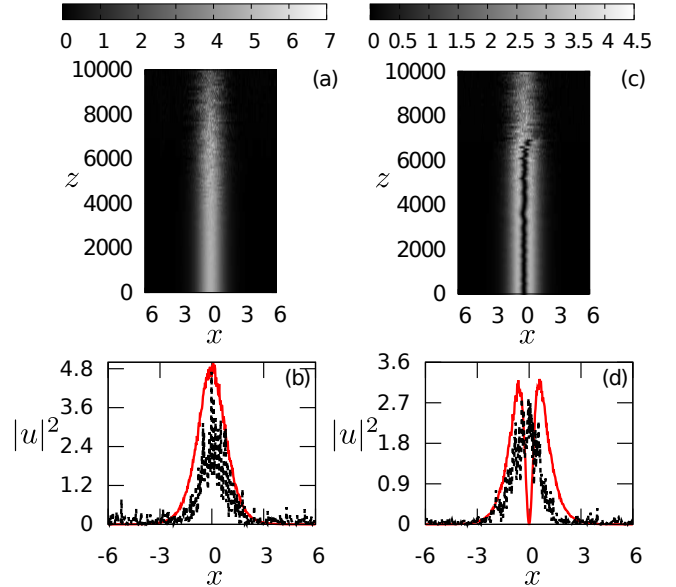


Figure 5: Upper panels show the unstable evolution of the modes with $\alpha = 1.7$, while the lower panels display the comparison between the density of the initial state at $z = 0$ (solid lines) and in the output at $z = 10000$ (dotted lines). The initial powers are $P = 10$ for the nodeless mode u_0 in (a,b), and $P = 7$ for the first excited mode u_1 in (c,d).

case, the evolution of the unstable nodeless mode leads to a power loss of 28.9% by $z = 10^4$, induced by the boundary absorbers. The evolution and comparison between the input and output profiles are shown in Figs. 5(a,b). Somewhat similar evolution of the first-order mode u_1 is reported in Figs. 5(c,d), for $\alpha = 1.7$ and $P = 7$. The evolution of this input produces a 24.3% power loss and ends up by the spontaneous transformation into a nodeless single-shape profile. A general trend is towards rearrangement of the unstable nodeless state into a stable one with a smaller power.

Finally, Fig. 6 summarizes results of this work in the form of stability charts for modes u_0 , u_1 and u_2 in the parameter plane (P, α) . We observe that the nodeless state is fully stable, as may be expected from the ground state, for all values of the power in a broad interval of the LI values, $0.3 < \alpha < 1.6$, as well as in a narrow one,

$$1.7 < \alpha < 1.9. \quad (17)$$

When the nodeless modes are unstable, they tend to evolve with power losses, as shown above. The dynamics of the first excited mode, u_1 , are quite different, but they share the stability interval (17) with the nodeless mode. Finally, no stability region was found for the second-order mode, u_2 .

4. Conclusion

We have demonstrated that the FNLSE (fractional nonlinear Schrödinger equation) with the trapping nonlinear potential, induced by the spatially modulated defocusing cubic nonlinearity, maintains stable self-trapped

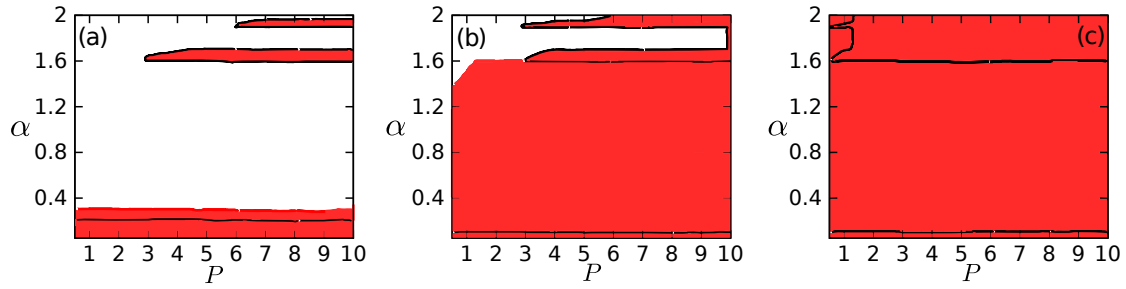


Figure 6: Stability charts for modes u_0 (a), u_1 (b) and u_2 (c). The solutions are stable and unstable in white and red regions, respectively. The areas delimited by the solid black line indicate instability regions where the solutions spontaneously transform into others with fewer nodes (eventually, into nodeless ones) and a lower norm.

modes. The model can be realized in a nonlinear planar waveguide with the effective fractional diffraction. The linear-stability analysis and direct simulations show that the nodeless modes, as well as the dipole single-node ones (the first excited state) have well-defined stability regions in the plane of the LI (Lévy index) and power. On the other hand, higher-order states featuring two or more nodes are never fully stable, spontaneously transforming into modes of lower orders. The instability-driven evolution leads to considerable power losses, caused by the use of the edge absorbers in the direct simulations, at higher values of LI, and to negligible losses at lower values. The numerical findings presented in this study suggest new possibilities for experimental realization of the predicted phenomenology.

A natural direction for the extension of the analysis is to develop it in the two-dimensional geometry with fractional diffraction. In that case, new options will be to construct vortex solitons and study their stability.

Declaration of competing interest

The authors declare that they have no known competing financial interests or personal relationships that could have appeared to influence the work reported in this paper.

Acknowledgments

M.C.P.S. and W.B.C. thank the financial support of the Brazilian agencies CNPq (#306105/2022-5) and CAPES. This work was also performed as part of the Brazilian National Institute of Science and Technology (INCT) for Quantum Information (#465469/2014-0). The work of B.A.M. was supported, in part, by grant No. 1695/22 from the Israel Science Foundation.

References

- [1] N. Laskin, [Fractional quantum mechanics and Lévy path integrals](#), *Phys. Lett. A* 268 (4-6) (2000) 298–305. doi:10.1016/S0375-9601(00)00201-2. URL <https://linkinghub.elsevier.com/retrieve/pii/S0375960100002012>
- [2] N. Laskin, [Fractional Schrödinger equation](#), *Phys. Rev. E* 66 (5) (2002) 056108. doi:10.1103/PhysRevE.66.056108. URL <https://link.aps.org/doi/10.1103/PhysRevE.66.056108>
- [3] N. Laskin, [Fractional Quantum Mechanics](#), WORLD SCIENTIFIC, 2018. doi:10.1142/10541. URL <https://www.worldscientific.com/worldscibooks/10.1142/10541>
- [4] Y. Hu, [Schrödinger Equations with Fractional Laplacians](#), *Appl. Math. Optim.* 42 (3) (2000) 281–290. doi:10.1007/s002450010014. URL <http://link.springer.com/10.1007/s002450010014>
- [5] B. B. Mandelbrot, [The fractal geometry of nature](#), Vol. 1, WH free-man New York, 1982.
- [6] O. P. Agrawal, [Fractional variational calculus in terms of Riesz fractional derivatives](#), *J. Phys. A Math. Theor.* 40 (24) (2007) 6287–6303. doi:10.1088/1751-8113/40/24/003. URL <https://iopscience.iop.org/article/10.1088/1751-8113/40/24/003>
- [7] M. Cai, C. Li, [On Riesz Derivative](#), *Fract. Calc. Appl. Anal.* 22 (2) (2019) 287–301. doi:10.1515/fca-2019-0019. URL <https://link.springer.com/10.1515/fca-2019-0019>
- [8] M. Jeng, S.-L.-Y. Xu, E. Hawkins, J. M. Schwarz, [On the nonlocality of the fractional Schrödinger equation](#), *J. Math. Phys.* 51 (6) (jun 2010). doi:10.1063/1.3430552. URL <https://pubs.aip.org/jmp/article/51/6/062102/232212/On-the-nonlocality-of-the-fractional-Schrodinger>
- [9] Y. Luchko, [Fractional Schrödinger equation for a particle moving in a potential well](#), *J. Math. Phys.* 54 (1) (jan 2013). doi:10.1063/1.4777472. URL <https://pubs.aip.org/jmp/article/54/1/012111/983786/Fractional-Schrodinger-equation-for-a-particle>
- [10] S. Duo, Y. Zhang, [Mass-conservative Fourier spectral methods for solving the fractional nonlinear Schrödinger equation](#), *Comput. Math. with Appl.* 71 (11) (2016) 2257–2271. doi:10.1016/j.camwa.2015.12.042. URL <https://linkinghub.elsevier.com/retrieve/pii/S0898122115006203>
- [11] L. P. Pitaevskii, S. Stringari, [Bose–Einstein Condensation](#), International Series of Monographs on Physics, Clarendon Press, 2003. URL <https://books.google.com.br/books?id=rIobb0xC4j4C>
- [12] B. A. Malomed, [Optical Solitons and Vortices in Fractional Media: A Mini-Review of Recent Results](#), *Photonics* 8 (9) (2021) 353. doi:10.3390/photonics8090353. URL <https://www.mdpi.com/2304-6732/8/9/353>
- [13] H. Sakaguchi, B. A. Malomed, [One- and two-dimensional solitons in spin-orbit-coupled Bose–Einstein condensates with fractional kinetic energy](#), *J. Phys. B At. Mol. Opt. Phys.* 55 (15) (2022) 155301. doi:10.1088/1361-6455/ac7685. URL <https://iopscience.iop.org/article/10.1088/1361-6455/ac7685>
- [14] B. A. Stickler, [Potential condensed-matter realization of space-fractional quantum mechanics: The one-dimensional Lévy crystal](#), *Phys. Rev. E* 88 (1) (2013) 012120. doi:10.1103/PhysRevE.88.012120.

- URL <https://link.aps.org/doi/10.1103/PhysRevE.88.012120>
- [15] F. Pinsker, W. Bao, Y. Zhang, H. Ohadi, A. Dreismann, J. J. Baumberg, Fractional quantum mechanics in polariton condensates with velocity-dependent mass, *Phys. Rev. B* 92 (19) (2015) 195310. doi:10.1103/PhysRevB.92.195310.
URL <https://link.aps.org/doi/10.1103/PhysRevB.92.195310>
- [16] Y. S. Kivshar, G. P. Agrawal, *Optical solitons: from fibers to photonic crystals*, Academic press, 2003.
- [17] S. Longhi, Fractional Schrödinger equation in optics, *Opt. Lett.* 40 (6) (2015) 1117. doi:10.1364/OL.40.001117.
URL <https://opg.optica.org/abstract.cfm?URI=ol-40-6-1117>
- [18] S. Liu, Y. Zhang, B. A. Malomed, E. Karimi, Experimental realisations of the fractional Schrödinger equation in the temporal domain, *Nat. Commun.* 14 (1) (2023) 222. doi:10.1038/s41467-023-35892-8.
URL <https://www.nature.com/articles/s41467-023-35892-8>
- [19] L. Zeng, J. Zeng, One-dimensional gap solitons in quintic and cubic-quintic fractional nonlinear Schrödinger equations with a periodically modulated linear potential, *Nonlinear Dyn.* 98 (2) (2019) 985–995. doi:10.1007/s11071-019-05240-x.
URL <http://link.springer.com/10.1007/s11071-019-05240-x>
- [20] J. Chen, J. Zeng, Spontaneous symmetry breaking in purely nonlinear fractional systems, *Chaos An Interdiscip. J. Nonlinear Sci.* 30 (6) (jun 2020). doi:10.1063/5.0006050.
URL <https://pubs.aip.org/cha/article/30/6/063131/287012/Spontaneous-symmetry-breaking-in-purely-nonlinear>
- [21] S. Secchi, M. Squassina, Soliton dynamics for fractional Schrödinger equations, *Appl. Anal.* 93 (8) (2014) 1702–1729. doi:10.1080/00036811.2013.844793.
URL <https://www.tandfonline.com/doi/full/10.1080/00036811.2013.844793>
- [22] M. Chen, S. Zeng, D. Lu, W. Hu, Q. Guo, Optical solitons, self-focusing, and wave collapse in a space-fractional Schrödinger equation with a Kerr-type nonlinearity, *Phys. Rev. E* 98 (2) (2018) 022211. doi:10.1103/PhysRevE.98.022211.
URL <https://link.aps.org/doi/10.1103/PhysRevE.98.022211>
- [23] C. Huang, L. Dong, Gap solitons in the nonlinear fractional Schrödinger equation with an optical lattice, *Opt. Lett.* 41 (24) (2016) 5636. doi:10.1364/OL.41.005636.
URL <https://opg.optica.org/abstract.cfm?URI=ol-41-24-5636>
- [24] J. Xiao, Z. Tian, C. Huang, L. Dong, Surface gap solitons in a nonlinear fractional Schrödinger equation, *Opt. Express* 26 (3) (2018) 2650. doi:10.1364/OE.26.002650.
URL <https://opg.optica.org/abstract.cfm?URI=oe-26-3-2650>
- [25] L. Dong, Z. Tian, Truncated-Bloch-wave solitons in nonlinear fractional periodic systems, *Ann. Phys. (N. Y.)* 404 (2019) 57–65. doi:10.1016/j.aop.2019.02.017.
URL <https://linkinghub.elsevier.com/retrieve/pii/S000349161930051X>
- [26] D. V. Strunin, B. A. Malomed, Symmetry-breaking transitions in quiescent and moving solitons in fractional couplers, *Phys. Rev. E* 107 (6) (2023) 064203. doi:10.1103/PhysRevE.107.064203.
URL <https://link.aps.org/doi/10.1103/PhysRevE.107.064203>
- [27] O. V. Borovkova, Y. V. Kartashov, L. Torner, B. A. Malomed, Bright solitons from defocusing nonlinearities, *Phys. Rev. E* 84 (3) (2011) 035602. doi:10.1103/PhysRevE.84.035602.
URL <https://link.aps.org/doi/10.1103/PhysRevE.84.035602>
- [28] O. V. Borovkova, Y. V. Kartashov, V. A. Vysloukh, V. E. Lobanov, B. A. Malomed, L. Torner, Solitons supported by spatially inhomogeneous nonlinear losses, *Opt. Express* 20 (3) (2012) 2657. doi:10.1364/OE.20.002657.
URL <https://opg.optica.org/oe/abstract.cfm?uri=oe-20-3-2657>
- [29] J. Zeng, B. A. Malomed, Bright solitons in defocusing media with spatial modulation of the quintic nonlinearity, *Phys. Rev. E* 86 (3) (2012) 036607. doi:10.1103/PhysRevE.86.036607.
URL <https://link.aps.org/doi/10.1103/PhysRevE.86.036607>
- [30] Q. Tian, L. Wu, Y. Zhang, J.-F. Zhang, Vortex solitons in defocusing media with spatially inhomogeneous nonlinearity, *Phys. Rev. E* 85 (5) (2012) 056603. doi:10.1103/PhysRevE.85.056603.
URL <https://link.aps.org/doi/10.1103/PhysRevE.85.056603>
- [31] Y. Wu, Q. Xie, H. Zhong, L. Wen, W. Hai, Algebraic bright and vortex solitons in self-defocusing media with spatially inhomogeneous nonlinearity, *Phys. Rev. A* 87 (5) (2013) 055801. doi:10.1103/PhysRevA.87.055801.
URL <https://link.aps.org/doi/10.1103/PhysRevA.87.055801>
- [32] W. B. Cardoso, J. Zeng, A. T. Avelar, D. Bazeia, B. A. Malomed, Bright solitons from the nonpolynomial Schrödinger equation with inhomogeneous defocusing nonlinearities, *Phys. Rev. E* 88 (2) (2013) 025201. doi:10.1103/PhysRevE.88.025201.
URL <https://link.aps.org/doi/10.1103/PhysRevE.88.025201>
- [33] R.-X. Zhong, Z.-P. Chen, C.-Q. Huang, Z.-H. Luo, H.-S. Tan, B. A. Malomed, Y.-Y. Li, Self-trapping under two-dimensional spin-orbit coupling and spatially growing repulsive nonlinearity, *Front. Phys.* 13 (4) (2018) 130311. doi:10.1007/s11467-018-0778-y.
URL <http://link.springer.com/10.1007/s11467-018-0778-y>
- [34] B. A. Malomed, D. E. Pelinovsky, Persistence of the Thomas–Fermi approximation for ground states of the Gross–Pitaevskii equation supported by the nonlinear confinement, *Appl. Math. Lett.* 40 (2015) 45–48. doi:10.1016/j.aml.2014.09.004.
URL <https://linkinghub.elsevier.com/retrieve/pii/S0893965914003061>
- [35] J. Hukriede, D. Runde, D. Kip, Fabrication and application of holographic Bragg gratings in lithium niobate channel waveguides, *J. Phys. D: Appl. Phys.* 36 (3) (2003) R1–R16. doi:10.1088/0022-3727/36/3/201.
URL <https://iopscience.iop.org/article/10.1088/0022-3727/36/3/201>
- [36] Y. V. Kartashov, B. A. Malomed, L. Torner, Solitons in nonlinear lattices, *Rev. Mod. Phys.* 83 (1) (2011) 247–305. doi:10.1103/RevModPhys.83.247.
URL <https://link.aps.org/doi/10.1103/RevModPhys.83.247>
- [37] J. Yang, *Nonlinear Waves in Integrable and Nonintegrable Systems*, Society for Industrial and Applied Mathematics, 2010. doi:10.1137/1.9780898719680.
URL <http://epubs.siam.org/doi/book/10.1137/1.9780898719680>
- [38] X. Antoine, W. Bao, C. Besse, Computational methods for the dynamics of the nonlinear Schrödinger/Gross–Pitaevskii equations, *Comput. Phys. Commun.* 184 (12) (2013) 2621–2633. doi:10.1016/j.cpc.2013.07.012.
URL <https://linkinghub.elsevier.com/retrieve/pii/S0010465513002403>
- [39] H. Sakaguchi, B. A. Malomed, Solitons in combined linear and nonlinear lattice potentials, *Phys. Rev. A* 81 (1) (2010) 013624. doi:10.1103/PhysRevA.81.013624.
URL <https://link.aps.org/doi/10.1103/PhysRevA.81.013624>
- [40] N. G. Vakhitov, A. A. Kolokolov, Stationary solutions of the wave equation in a medium with nonlinearity saturation, *Radiophys. Quantum Electron.* 16 (7) (1973) 783–789. doi:10.1007/BF01031343.
URL <http://link.springer.com/10.1007/BF01031343>
- [41] L. Bergé, Wave collapse in physics: principles and applications to light and plasma waves, *Phys. Rep.* 303 (5-6) (1998) 259–370. doi:10.1016/S0370-1573(97)00092-6.
URL <https://linkinghub.elsevier.com/retrieve/pii/S0370157397000926>
- [42] G. Fibich, *The Nonlinear Schrödinger Equation: Singular Solu-*

tions and Optical Collapse, Vol. 192 of Applied Mathematical Sciences, Springer International Publishing, Cham, 2015. doi:10.1007/978-3-319-12748-4.
URL <http://link.springer.com/10.1007/978-3-319-12748-4>